Fractal level sets and multifractal fields in direct simulations of turbulence

Axel Brandenburg and Itamar Procaccia
Department of Chemical Physics, The Weizmann Institute of Science, Rehovot 76100, Israel and NORDITA, Blegdamsvej 17, DK-2100 Copenhagen Ø, Denmark

Daniel Segel
Department of Chemical Physics, The Weizmann Institute of Science, Rehovot 76100, Israel

Alain Vincent
CERFACS, 42 Avenue Coriolis, F-31057 Toulouse, France
(Received 30 April 1992)

The fractal nature of level sets and the multifractal nature of various scalar and vector fields in hydromagnetic and hydrodynamic turbulence are investigated using data of direct simulations. It turns out that fields whose evolution is governed by stretching terms (vortex stretching, magnetic-field line stretching) exhibit "near singularities" that result in a multifractal scaling. Such stretching terms can lead to a rapid increase in the local value of the field. Fields without rapid local increase have no multifractal scaling. Furthermore, the simulations support recent theoretical suggestions that the fractal properties of the *level sets* of various fields are quite insensitive to the existence of stretching. Indeed, all the fields under study (temperature, vorticity magnitude, magnetic-field magnitude) show rather universal behavior in the geometry of their level sets, consistent with a two-dimensional geometry at small scales, with a crossover to a universal fractal geometry at large scales. The dimension at large scales is compatible with the theoretical prediction of about 2.7. The most surprising result of the simulations is that it appears that the "near singularities" are not efficiently eliminated by viscous dissipation, but rather seem to be strongest at the Kolmogorov cutoff. The effects of the singularities do not quite penetrate into the inertial range. We offer a simple analytic model to account for this behavior. We conclude that our findings may be due to the relatively small Reynolds numbers, but may also be indicative of generic behavior at larger Reynolds numbers. We offer some thoughts about the expected scaling behavior in the inertial range in light of our findings.

PACS number(s): 47.25.−c

I. INTRODUCTION

If turbulence possesses universal properties, they are most likely to be manifested in the scaling behavior of correlation and structure functions in the inertial range. Unfortunately, the scaling behavior of turbulence is still ill understood beyond the phenomenological Kolmogorov picture. However it is felt by many that insight into the scaling behavior can be gained by understanding the geometrical structures in turbulence, including their fractal and multifractal properties. If these turned out to be universal, light might be shed on the question of the universal scaling behavior of statistical quantities like the structure functions. Obviously, it would be most profitable to study the geometrical issues directly on the basis of the equations of fluid mechanics. Recently, the fractal nature of level sets has been studied on the basis of fluid mechanics with the aid of ideas from geometric measure theory [1]. It has been shown that there exists a degree of universality in the sense that all the fields studied, be they "passive" or "active," exhibit a crossover from smooth to fractal behavior with a dimension that can be bounded by a universal estimate.

On the other hand, all the theoretical studies concerning the multifractal nature of turbulent fields have been limited so far to rather contrived models or phenomenological guesses. It would be worthwhile to attempt to connect the existence or nonexistence of multifractal scaling to the underlying equations of motion. In this paper we take the point of view that the crucial aspect in the equation of motion is whether the field in question can be rapidly amplified locally so as to create a singularity. We are aware of the elusive nature of the singularities in fluid mechanics, and nowhere in this paper do we claim to have found a "real" singularity of the type discussed by Cafarelli, Kohn, and Nirenberg [2]. We shall show however that direct simulations indicate very strongly that fields governed by a rapid local stretching have fundamentally different scaling properties from fields that lack such local stretching. From the point of view of the generalized dimensions it appears that there exist "near singularities" in those fields that are rapidly stretched.

Our naive expectation had been that if a near singularity were developing it would be felt mostly in the inertial range, and that it would be smoothed out by viscous effects on the Kolmogorov cutoff scale. To our surprise we see quite the opposite. It seems that viscous effects are inefficient in taming the near singularities which seem quite apparent in the viscous range. The model that seems demanded by the data is of a rather smooth back-

ground on which near singularities of a rather small amplitude are riding. The multifractal analysis picks out the effect of the singularities only at small scales. Below we shall offer a simple analytic model that captures the qualitative scaling properties that we see in the data. The consequences of this model for the scaling behavior in the inertial range are discussed below.

In the following we shall distinguish between the fractal dimension D of the level sets and the generalized dimensions D_q of the fields themselves. The former concept is connected in a simulation to finding all the points in space for which the value of a chosen field falls within a prescribed window, and then to computing the dimension of this set of points. The latter quantities are computed by boxing space into boxes of size r, and integrating a chosen field in every such box. Normalizing, one gets the "measure" of each box of size r, and then computes the generalized dimensions as usual. (Precise definitions and procedures are provided in Secs. III and IV.) It has been pointed out before that the generalized dimensions differ from the embedding dimension only if the fields contain singularities. The computation of these quantities is therefore a convenient tool to assess the existence of large variations in the magnitudes of the measure from point to point.

There have been various attempts to quantify the fractal nature of turbulent flows in the laboratory. For several types of turbulent flows Meneveau and Sreenivasan [3] and Prasad, Meneveau, and Sreenivasan [4] estimated the generalized dimensions D_q of the dissipation field from a time series. Constantin, Procaccia, and Sreenivasan [5] found the dimension of isoconcentration surfaces for a passive scalar using spatially resolved two-dimensional dye images.

Recently, the fractal dimension of isovorticity surfaces in hydrodynamic turbulence has been estimated both analytically [1] and from numerical simulations [6]. There is generally a crossover at some intermediate scale (about ten Kolmogorov dissipation lengths) from a two-dimensional geometry at small scales to $D = 2.5 + \zeta/2$ at large scales, where ζ is the scaling exponent of the velocity differences. This shows that while at small scales isovorticity surfaces are smooth structures, at large scales these surfaces are more and more wrinkled, giving rise to a fractal dimension larger than 2.

Because of the close analogy between the vorticity equation and the induction equation, the same methods and ideas should carry over to the case of magnetohydrodynamic (MHD) turbulence. The analogy between the equations governing the evolution of the vorticity $\mathbf{w} = \boldsymbol{\nabla} \times \mathbf{u}$ in ordinary hydrodynamics (in the absence of magnetic fields, gravity, and rotation) and magnetic field $\mathbf{B}$ in MHD has often been helpful: in the context of MHD turbulence, for example, Batchelor [7] used this analogy to explain the possibility of spontaneous magnetic field generation (the dynamo effect). Numerical simulations of homogeneous three-dimensional Navier-Stokes turbulence have revealed that the turbulent flow is organized in the form of thin, elongated vortex tubes with a length close to the integral scale and a typical thickness of the order of a few Kolmogorov dissipation scales [8, 9]. In numerical simulations of MHD turbulence, magnetic flux tubes, analogous to vortex tubes in ordinary hydrodynamic turbulence, have been observed [10, 11], thus substantiating the close analogy between $\mathbf{w}$ and $\mathbf{B}$.

A fractal analysis of hydrodynamic and MHD turbulence has direct astrophysical applications because the flow pattern (e.g., the granulation) and the magnetic field on the solar surface seem to exhibit a fractal nature that has been studied in recent years [12, 13]. Different explanations have been offered for the fractal dimension of the solar magnetic field at the surface including, for example, a nonuniformity of the stretch-twist-fold dynamo mechanism [14], and a random occurrence of magnetic fields has been described by percolation theory [15]. Similarly, the flows on scales of mesogranules have been modeled by random processes and the fractal dimension of a set of advected tracers has been estimated [16]. These approaches remain unsatisfactory in that they ignore the dynamical evolution of the velocity and the magnetic field as governed by the MHD and Navier-Stokes equations.

Here we analyze the data for homogeneous turbulence of Vincent and Meneguzzi [9] with a resolution of 240^3 Fourier components, and for convective MHD turbulence of Nordlund *et al.* [11] with a resolution of 63^3 meshpoints. In the first case the flow is driven by a constant forcing at large scales, whereas in the latter turbulent convection develops from a constant heat flux imposed at the bottom of a plane layer and cooling above. In addition, we also analyze the data of a run of decaying turbulence performed by Vincent and Meneguzzi [17] using 256^3 Fourier components. Here, the Reynolds number is smaller (140 instead of $\sim$ 1000) and the Kolmogorov cutoff better resolved than in the run for forced turbulence. The MHD simulation is tailored to describe the flow and the magnetic fields in deeper layers of the Sun, and therefore a number of physical features are included, such as rotation and density stratification. Furthermore, the lower half of the layer is stably stratified allowing penetration from above. Since the dynamics in this lower layer is much less chaotic, we exclude it from the subsequent analysis. The magnetic diffusivity is sufficiently small so that a weak seed magnetic field is amplified, until saturation is reached, where kinetic and magnetic energies are almost in equipartition. The physical parameters of this run are Rayleigh number 10^6, Taylor number 10^5, Prandtl number 0.2, and magnetic Prandtl number 4, and the Reynolds number fluctuates around 300; see Ref. [11].

By comparing the data sets of hydrodynamic and MHD turbulence we may get some feeling as to what extent our results are sensitive with respect to such additional physics. Furthermore, since the numerical methods employed in the two cases are different (spectral and mesh point methods, respectively) we have an additional check on the numerical reliability of the data presented.

II. EVOLUTION EQUATIONS AND STRETCHING

In this section we discuss the equations of motion of the various fields that are available in the MHD simulation,

displaying their similarities and differences. In particular it is important to point out the significant role of the stretching terms $w_j\partial_j u_i$ and $B_j\partial_j u_i$ that occur on the right-hand side of the vorticity and induction equations [7]. The equation for the magnitude of the magnetic field, $B = |\mathbf{B}|$, can be written in the form

$$\frac{\partial B}{\partial t} + \mathbf{u}\cdot\boldsymbol{\nabla}B - \eta\boldsymbol{\nabla}^2 B = f_B B, \tag{1}$$

where $f_B = \hat{B}_i\hat{B}_j s_{ij} - \eta(\partial_j\hat{B}_i)^2 - \nabla\cdot\mathbf{u}$ and $\hat{B}_i = B_i/B$ are the components of the unit vector in the direction of $\mathbf{B}$. Here, only the symmetric part s_{ij} of the velocity gradient matrix enters, where s_{ij} is the usual rate of strain tensor

$$s_{ij} = \tfrac{1}{2}(\partial_i u_j + \partial_j u_i). \tag{2}$$

The same equations are obeyed by the vorticity magnitude $w = |\mathbf{w}|$ in hydrodynamics (without gravity and stratification), except for the additional constraint $\mathbf{w} = \boldsymbol{\nabla}\times\mathbf{u}$; for $\mathbf{B}$ there is no such condition.

Using this form of the equation, the dimension of the level sets of these fields can be found using the analytic methods developed by Constantin and Procaccia [1]. We thus expect a crossover behavior in the computed dimension, where the crossover is from $D = 2$ to $D = 2.5+\zeta/2$, occurring at a typical scale λ^* which is about one order of magnitude larger than the Kolmogorov cutoff scale. For $\zeta \approx 0.4$ the dimension at large scales is expected to be about 2.7.

In the equations like those for the velocity and temperature fields, stretching terms are absent. For a compressible, perfect gas the equation for the temperature T is

$$\frac{\partial T}{\partial t} + \mathbf{u}\cdot\boldsymbol{\nabla}T - \kappa\nabla^2 T = f_T T + \cdots, \tag{3}$$

where $f_T = -(\gamma-1)\boldsymbol{\nabla}\cdot\mathbf{u}$, γ is the ratio of the specific heats ($=\frac{5}{3}$ in our case), and $\kappa = K/\rho$ is the heat diffusion coefficient, where K is a constant and ρ is density. The dots on the right-hand side of (3) denote viscous and Joule heat terms, which do not explicitly depend on T.

Note that (3) is of similar form to (1), except for the structure of the terms f_B and f_T on the right-hand side. In the two equations these terms can cause a local exponential increase or decay of B (or T), depending on the sign of f_B (or f_T). On the average, however, the stretching terms in the vorticity and induction equations are always positive [7], while the corresponding term on the right-hand side of Eq. (3), namely, $-T\boldsymbol{\nabla}\cdot\mathbf{u}$, gives a strongly negative contribution on the average (see below).

The magnitude of the gradient of the temperature $\beta = |\boldsymbol{\nabla}T|$ satisfies

$$\frac{\partial\beta}{\partial t} + \mathbf{u}\cdot\boldsymbol{\nabla}\beta - \kappa\boldsymbol{\nabla}^2\beta = f_\beta\beta + \cdots, \tag{4}$$

where $f_\beta = -\hat{\beta}_i\hat{\beta}_j s_{ij} - \kappa(\partial_j\hat{\beta}_i)^2 - (\gamma-1)\boldsymbol{\nabla}\cdot\mathbf{u}$. The ellipsis on the right-hand side of (4) denotes terms arising from the density gradient and the viscous and Joule heat terms. Note that f_β also has a stretching term, $-\hat{\beta}_i\hat{\beta}_j s_{ij}$, and it is therefore interesting to compare the multifractal behavior of B and β. However, the stretching term in f_β has the opposite sign to that in f_B and we may therefore expect that this term gives a negative contribution on the average, so that the β field would not show multifractality. Nevertheless, we cannot exclude *a priori* the possibility that there is generation of near singularities in β, even though there is no exponential growth of the temperature gradient on the average. Indeed, it has been found in other contexts that the gradient of a passive scalar can exhibit a multifractal behavior, see, for example, Ramshankar and Gollub [18]. Below, we show that in our context of low Prandtl number convection the stretching of the temperature gradient is not strong enough to develop multifractality.

Note that the T and β fields are dominated by a stratification component which varies slowly with depth. It is therefore reasonable to consider instead $\beta' = \nabla T'$, where T' denotes the deviation of T from the average stratification. The equations for T' and β' have similar terms on the right-hand side to (3) and (4), and the same arguments therefore apply. We recall that the simulation results used here are obtained by solving the full equations, and T' and β' are then obtained by subtracting the average stratification.

In order to describe the nature of the stretching terms further, we show in Fig. 1 histograms of the probability density functions of $S_w = w_i w_j s_{ij}$, $S_B = B_i B_j s_{ij}$, $S_{\beta'} = \beta'_i\beta'_j s_{ij}$, and $T'\boldsymbol{\nabla}\cdot\mathbf{u}$. The kurtosis of these distribution functions is rather high (390, 190, 220, and 16, respectively), indicating that stretching comes from only a few burstlike events. The skewness of the four distributions is positive (12, 4.7, 5.3, and 3.3, respectively), indicating that large positive contributions are clearly more probable than negative ones, and that positive values of $T'\boldsymbol{\nabla}\cdot\mathbf{u}$ are far more probable than negative values. Since both $T'\boldsymbol{\nabla}\cdot\mathbf{u}$ and $S_{\beta'}$ occur with a minus sign in Eqs. (3) and (4), respectively, we conclude that local exponential growth in T' and β' cannot be dominant.

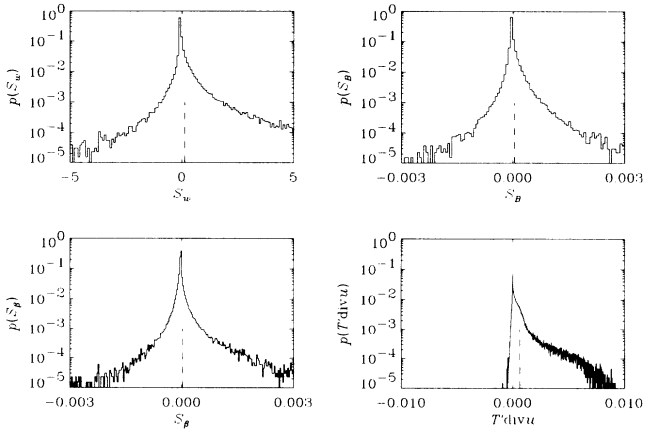

FIG. 1. Histograms of the probability density functions of $S_w = w_i w_j s_{ij}$, $S_B = B_i B_j s_{ij}$, $S_{\beta'} = \beta'_i\beta'_j s_{ij}$, and $T'\boldsymbol{\nabla}\cdot\mathbf{u}$. The average is indicated by a dashed vertical line.

III. LEVEL SETS

Using the technique described in Procaccia *et al.* [6] we first consider, for the MHD case, the fractal dimensions of level sets of T', w, and B. We select a narrow window and produce in this way a set of about 4000 points. We then compute the correlation integral $C(r)$ giving the number of pairs of points whose distance is less than or equal to r. $D(r)$ is then obtained as the pointwise slope of $\ln C$ versus $\ln r$. For T', w, and B we find that $D(r)$ is compatible with a crossover from 2 at small scales to 2.7 at large scales, which is in agreement with previous results for homogeneous turbulence; see Fig. 2. We checked that similar results were obtained for different levels and widths of the window. Notwithstanding, we should point out that $D(r)$ has a tendency to increase along much of the inertial range and the plateau at 2.7 is rather small. The same is true for the hydrodynamic case (see Fig. 2 in Ref. [6]). Thus, before having examined data at considerably higher Reynolds numbers and much larger inertial ranges, we cannot rule out the unpleasant possibility that the points belonging to the level sets are simply randomly distributed at the largest scales. If so, one would simply see a crossover behavior between two- and three-dimensional scaling. The fact that we do not reach $D(r) = 3$ even at the highest scales supports the feeling that this worry should not be taken too seriously into account.

IV. GENERALIZED DIMENSIONS

In the following we focus on the multifractal structure of various fields. The term f_B in Eq. (1) can have both signs, creating exponential growth at those points where it is positive. Fields whose evolution is governed by such a term can develop near singular structures, giving rise to a multifractal nature of these fields, i.e., generalized dimensions D_q that are smaller than 3 for $q > 0$.

Here, we investigate the generalized dimensions D_q [19] both for convective MHD turbulence and homogeneous turbulence. We use the box-counting algorithm to compute the generalized correlation integral

$$C_q(r) = \sum_i p_i^q, \tag{5}$$

where p_i is the weight, or normalized average field strength, in the ith box V_i with size r. For the B field, for example, we have

$$p_i = \int_{V_i} B\, d^3x \Big/ \int_V B\, d^3x, \tag{6}$$

where V is the total box size. In practice we evaluate (5) in the form

$$\frac{1}{q-1}\ln C_q(r) = \begin{cases} \dfrac{1}{q-1}\left(q\ln p_{\min} + \ln\sum_i (p_i/p_{\min})^q\right) & \text{for } q<0, \\ \dfrac{1}{q-1}\left(q\ln p_{\max} + \ln\sum_i (p_i/p_{\max})^q\right) & \text{for } q>0, \\ \ln p_{\min} \quad \text{for } q\to-\infty, \\ \ln p_{\max} \quad \text{for } q\to+\infty, \\ \sum_i p_i \ln p_i \quad \text{for } q=1, \\ -\ln\sum_i 1 \quad \text{for } q=0. \end{cases} \tag{7}$$

The r-dependent values of D_q can now be calculated from the slopes of $C_q(r)$ in a log-log plot, i.e.,

$$D_q(r) = \frac{1}{q-1}\frac{d\ln C_q}{d\ln r}. \tag{8}$$

The singularity spectrum $f(\alpha)$ can then be calculated from D_q using

$$f(\alpha) = q\alpha(q) - \tau(q), \quad \alpha(q) = \frac{d\tau}{dq}, \tag{9}$$

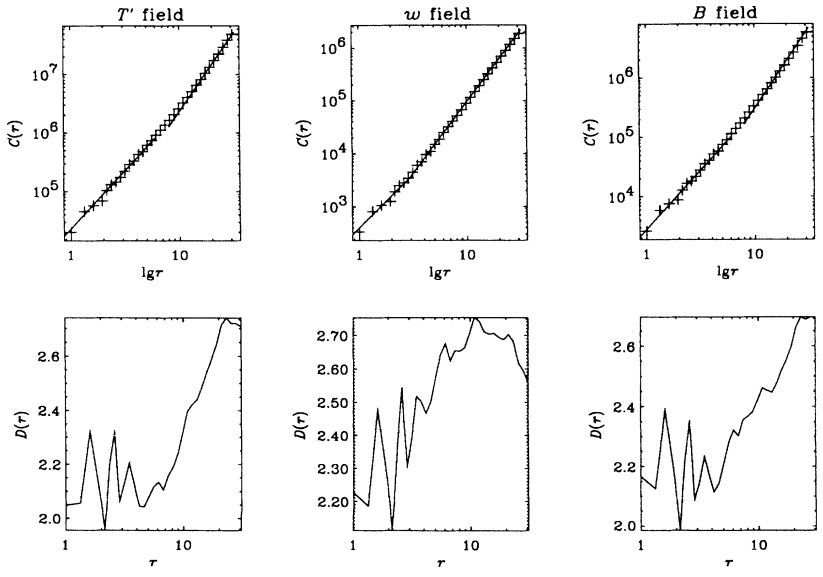

FIG. 2. Correlation integral (upper row) and correlation dimension (lower row) of level sets of T', w, and B for MHD convection. The straight lines in the upper three panels are fits with slopes 2 at small scales and 2.7 at large scales. r is in units of the mesh size.

where $\tau(q) = (q-1)D_q$ [20]. The $f(\alpha)$ representation is equivalent to the D_q representation because of the Legendre transform (9). It furnishes a feeling about the range of different local scaling exponents α and their density of occurrence. The higher f is for a certain value of α, the higher is the probability of finding this scaling exponent, and vice versa. It should be stressed at this point that in the computations performed here there is no control over the convergence of the $f(\alpha)$ curves. It is known from experience in other fields in which multifractal behavior has been found that the computation of the $f(\alpha)$ function is far from trivial. Before we learn to control the calculation all the results should be considered preliminary and taken as an indication only.

V. MULTIFRACTALITY

A. Numerical results

There are two aspects of the results that we describe next that we find most interesting. Firstly, the fields that we looked at fall into two different classes from the point of view of their multifractal scaling behavior: fields with strong stretching show distinct multifractality, whereas fields that are not strongly stretched show essentially no multifractality. Secondly, the multifractal behavior is best seen in the dissipative rather than the inertial range. This has come as a surprise for us.

We first present the results for pure hydrodynamics. The simulation in this case is such that the smallest resolved scale is the Kolmogorov cutoff scale. The value of D_1 of the w field shows a pronounced crossover from 2.7 at small scales to 3 at large scales; see Figs. 3 and 4. The fact that the D_q's for various values of q are clearly different from each other shows the multifractal structure of the w field, and indicates the presence of near singularities in w. Note that the D_q's remain strongly differentiated at the Kolmogorov cutoff scale, the lowest scale that this data reaches. This implies that if the values of D_q are indeed caused by near singularities, then these remain well defined even at these scales. In contrast, for

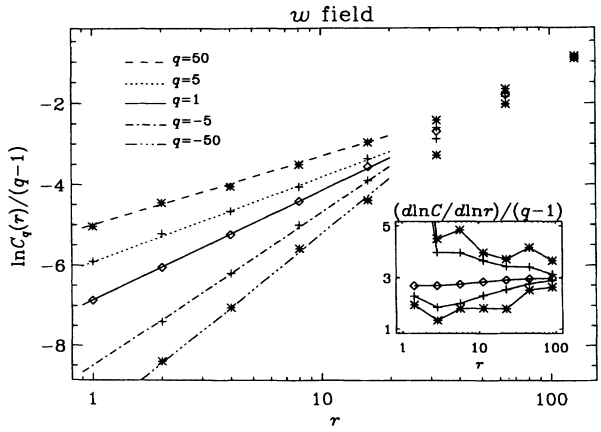

FIG. 3. $C_q(r)$ for $q = \pm 50$, ± 5, and $+1$ for forced homogeneous turbulence. The inset shows the r-dependent values of the dimension.

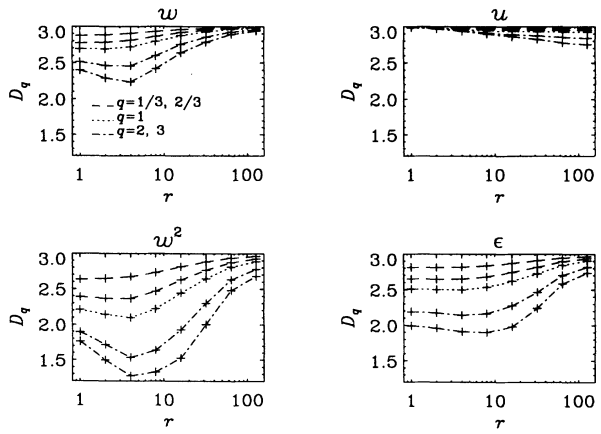

FIG. 4. Summary of $D_{1/3}$, $D_{2/3}$, D_1, D_2, and D_3 of w, u, w^2, and ε for forced homogeneous turbulence. The key to the lines is given in the first panel.

the velocity field, $u = |\mathbf{u}|$, all D_q's are 3, although at large scales there is a weak crossover to values somewhat smaller than 3. This latter feature can be caused by the presence of a large-scale flow that gives rise to considerable variations of p_i for large r.

Two fields that are of primary interest in the multifractal picture of turbulence are the local rate of energy dissipation $\varepsilon(\mathbf{x}) \propto s_{ij}^2$ and the square of the vorticity magnitude w^2. The idea to account for intermittency effects by replacing the average dissipation rate $\varepsilon = \langle \varepsilon(\mathbf{x}) \rangle$ by the local one [21] could also be justified if one took w^2 instead of $\varepsilon(\mathbf{x}) \propto s_{ij}^2$, because $2\langle s_{ij}^2 \rangle = \langle w^2 \rangle$. Here, angular brackets denote the average over the total volume. It is therefore useful to consider both fields. In some cases we confirmed that the pointwise fields s_{ij}^2 and w^2 look rather different. The two last panels in Fig. 4 show the r dependence of D_q for these two fields. For w^2 the information dimension levels off at $D_1 \approx 2.2$ for the smallest scales, while for ε this value is more like 2.5. Thus, at the smallest scales there is a clear difference in the multifractal scaling of the two fields. In fact, Kida and Ohkitani [22] have shown that the regions of large dissipation are typically concentrated *around* vortex tubes (see also Ref. [17]), which seems to be consistent with our result that $3 - D_1$ is smaller for the dissipation field than for the w^2 field. Since here we do not find good scaling in the inertial range, we do not know whether this difference indicates anything about the relevance of either field to the standard ideas about multifractal corrections to the inertial range scaling exponents. It is possible that at much higher Reynolds numbers the multifractal scaling that we find here at small scales penetrates more efficiently into the inertial range. The model that we shall develop in Sec. V B suggests this possibility rather strongly, but at this point we cannot be sure.

Figure 5 shows the q dependence of the generalized dimensions and the singularity spectrum $f(\alpha)$ for w^2 and ε. In this graph the solid line is obtained by solving Eq. (9) using for D_q an average over the values at $r = 2$, 4, 8, and 16 mesh sizes. The + signs denote the results for D_q

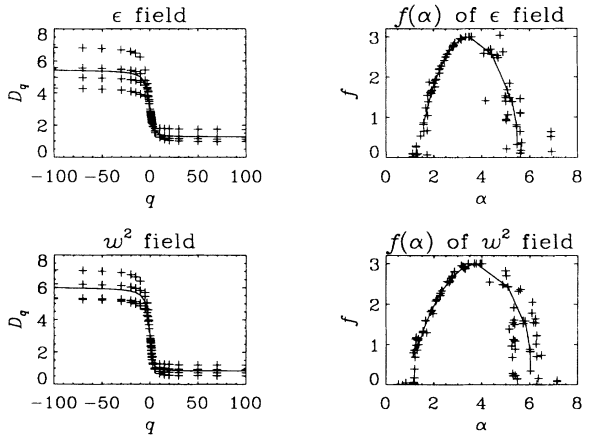

FIG. 5. D_q vs q (left panels) and $f(\alpha)$ spectrum (right panels) for ε and w^2 in forced homogeneous turbulence.

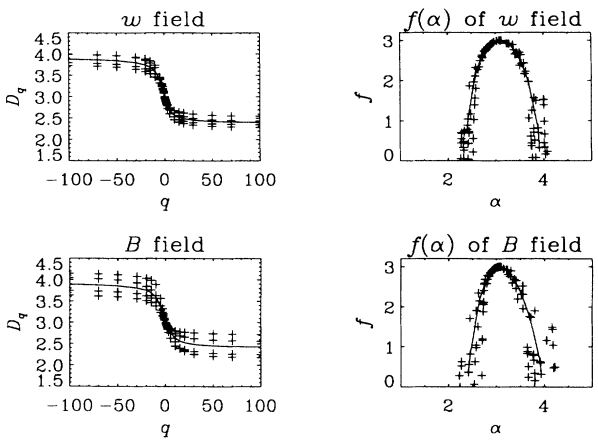

FIG. 7. D_q vs q (left panels) and $f(\alpha)$ spectrum (right panels) for w and B in MHD convection.

and $f(\alpha)$ obtained at these r values without averaging, giving some impression of the maximal scatter.

In MHD convection the B field shows a similar trend to the w field in the hydrodynamic case, but here the crossover is less strong: for example, D_1 varies only from 2.9 to 2.95; see Fig. 6, where we show $D_q(r)$ of w, w^2, u, β', B^2, and the Joule dissipation density J^2, where $J = |\mathbf{J}|$ and $\mathbf{J} = \nabla \times \mathbf{B}/\mu_0$ is the electric current. Nevertheless, both the w and B fields show a clear multifractal structure for small r. Here too, the multifractal structure persists down to the smallest scales. In this MHD simulation the Kolmogorov cutoff is not as well resolved as in the case of homogeneous turbulence. This may be part of the reason why the D_q's of our MHD data are, at small scales, less clearly differentiated than those of homogeneous turbulence. For the density and temperature fields we find that all dimensions are close to 3. This indicates that there are no singularities present in these fields, which is to be expected in the absence of strong stretching terms. The q dependence of D_q and the singularity spectrum $f(\alpha)$ of the w and B fields are shown in Fig. 7.

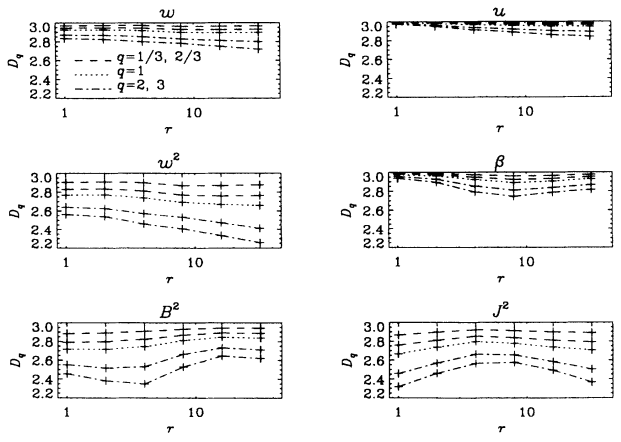

FIG. 6. Summary of $D_{1/3}$, $D_{2/3}$, D_1, D_2, and D_3 for w, u, w^2, β, B^2, and J^2 in MHD convection. The key to the lines is given in the first panel.

Both the velocity and the temperature gradient fields show a crossover from $D_1 \approx 3$ at small scales to somewhat smaller values at large scales; see Fig. 6. This confirms that these fields do not possess near singularities. Again, at large scales D_1 decreases somewhat, which indicates that there is a large-scale variation in these fields. The same trend is also seen in the w field. This is not surprising, because in convection with strong density stratification there is a large-scale flow, and typically a few strong downdrafts, that contribute to the nonuniformity of p_i for large r. This argument also applies to the w field in convection, where the Coriolis force sets the downdrafts into rapid rotation and thereby produces intense vertical vortex tubes that contribute to inhomogeneity at large scales. This explains the observed crossover towards smaller D_q in the w data for convection.

We cannot expect that the dimensions estimated for the level sets will coincide with the D_1 of the field, because the level set data indicate the degree of wrinkling and connectivity at larger scales, whereas the results of D_1 give information about the structures (singularities) at small scales. Nevertheless, since D_1 is the dimension of the points representing "most" of the field, one might expect [1] a correspondence with the isoset dimension if most of the field is concentrated about the singular structures. In fact, when comparing D_1 of w^2 for hydrodynamic turbulence (Fig. 4) and of w^2, B^2, J^2 for MHD (Fig. 6) we see that, for large values of r, D_1 is actually compatible with the value 2.7.

Our results of a crossover in the scaling of the dissipation field are in good qualitative agreement with the experimental measurements by Sreenivasan, although there one considers only a one-dimensional cut through the data.

B. A simple analytic model

In order to try to understand the results presented in Sec. V A we consider now an elementary model in which a

field $A(x)$ which takes values on a one-dimensional space has a "typical" background value b, on top of which a singularity is riding:

$$A(x) = ax^{\alpha-1} + b, \tag{10}$$

with $\alpha < 1$. For simplicity we shall take x to be in the unit interval $[0, 1]$, and the singularity is at the origin $x = 0$. The constants a and b are free except that $A(x)$ is taken to be normalized on the unit interval, i.e., $a/\alpha + b = 1$. The aim of the exercise is to see at what length scale (as a function of a/b) the generalized dimensions become sensitive to the existence of the singularity.

The procedure for calculating D_q starts with integrating the field on boxes of size r. We box the unit interval into $1/r$ such boxes, and integrate

$$p_i = \int_{ir}^{(i+1)r} A(x)dx \approx \begin{cases} ar^\alpha i^{\alpha-1} + br & \text{for } i \neq 0 \\ ar^\alpha + br & \text{for } i = 0. \end{cases} \tag{11}$$

The two terms in Eq. (11) are comparable when the index i takes the value i_c,

$$i_c = (a/b)^{1/(1-\alpha)} r^{-1} \equiv \xi/r. \tag{12}$$

Obviously, for $i < i_c$ the singularity dominates the value of p_i whereas for $i > i_c$ the background dominates the value of p_i. We can proceed now to evaluate the generalized dimensions

$$\begin{aligned} \sum_{i=0}^{1/r} p_i^q &\approx a^q r^{\alpha q} \left(1 + \sum_{i=1}^{i_c} i^{-Q}\right) + \sum_{i=i_c}^{1/r} b^q r^q \\ &\approx a^q r^{\alpha q} \left(1 + \int_1^{\xi/r} y^{-Q} dy\right) + b^q r^{q-1}(1-\xi) \\ &= r^{\alpha q} \frac{a^q}{1-1/Q} + r^{q-1}\left[\frac{a^q \xi^{1-Q}}{1-Q} + b^q(1-\xi)\right], \end{aligned} \tag{13}$$

where $Q = q(1-\alpha)$. Here we have only considered values of q such that $1 - Q < 0$. (For smaller q the effect of the singularity is not felt at any value of r.) The two terms on the right-hand side of (13) are comparable at a length scale r_c which, for $a \ll b$, is

$$r_c \approx [(a/b)^q (1 - 1/Q)]^{1/(Q-1)}. \tag{14}$$

The weaker the singularity, the smaller r_c becomes. For $r > r_c$ the effect of the singularity is unfelt, and the generalized dimensions would be all $D_q = 1$. For $r < r_c$ the singularity dominates and the generalized dimensions would be $D_q = \alpha q/(q-1)$, cf. Eq. (8).

The upshot of this calculation is that if indeed we have rather weak singularities riding on a uniform background, we begin to measure the generalized dimension only on small scales, and these depend on the relative amplitude of the singularity compared to the background. Notice that r_c increases with q (i.e., the singularities become progressively dominant at larger r as q increases), but r_c does not exceed a q-independent limit which is $(a/b)^{1/(1-\alpha)}$. It appears that the behavior presented in our figures is qualitatively in accord with this picture. Of course, we do not necessarily believe that there is only one singularity at any time in our data, but the general features are probably preserved in more general situations.

Obviously, one immediate prediction is that if the amplitude of the singularities increases when the Reynolds number goes up, then, since the Kolmogorov cutoff goes down, r_c must eventually get into the inertial range. Thus, if our simple model has anything to do with reality, we can predict that for high Reynolds numbers the effect of the singularities would be felt in the scaling properties of the inertial range. It is very likely however that for realistic values of the Reynolds number the scaling properties at sufficiently large scales (in the inertial range) would be consistent with pure Kolmogorov scaling, and only for smaller scales (still in the inertial range) the effects of the singularities would begin to change the scaling exponents. The smaller q is, the longer the range of pure Kolmogorov scaling is. When q increases, anomalous scaling can be seen sooner.

Finally, we want to examine the other possible crossover in the theory, i.e., at very small scales. As mentioned before, in the steady-state simulations we do not see any crossover even at the smallest scales. It is reasonable to assert that if one stopped forcing the system, the very small scales would be tamed first by the viscosity, and the "near singularity" would become less and less singular on the smallest scales. In such a case one would expect that the multifractal analysis would pick up a second crossover at small scales back to trivial values $D_q = 3$. In order to check this we have analyzed the data of a recent run of decaying turbulence performed by Vincent and Meneguzzi [17]. In the last snapshot of this run the Reynolds number had decreased to about 140 and the Kolmogorov cutoff is now resolved by a few mesh zones. The resulting dependence of D_q on r is shown in Fig. 8. There is now a clear tendency that $D_q(r) \to 3$ as $r \to 0$, which is in agreement with our expectations. Moreover, the minimal values of $D_q(r)$ are similar in both forced and decaying turbulence. This indicates that the strength of the near singularities is independent of the Reynolds number. This result may also enhance the reliability of the simulation of forced turbulence where the singularities are only marginally resolved. Therefore we expect that the phenomenon of the near singularities of the w^2 and ε fields is not going to disappear as the Reynolds number is increased further.

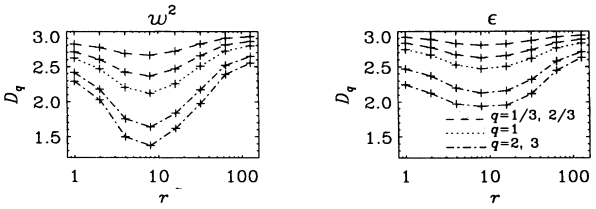

FIG. 8. Summary of $D_{1/3}$, $D_{2/3}$, D_1, D_2, and D_3 of w^2 and ε for decaying homogeneous turbulence. The key to the lines is given in the second panel.

VI. SINGULARITIES

It is interesting to find out whether the standard view that connects the existence of nontrivial generalized dimensions D_q to the influence of singularities is supported by the data. Peaks in the various fields are only resolved up to a few mesh zones, and it is therefore important to check whether possible near singularities are well resolved by the mesh. We would expect the strongest singularities to determine D_∞, so that the strongest peak in our data might be fitted to a functional form $|\mathbf{r}-\mathbf{r}_0|^{\tilde{\alpha}-3}$, with $\tilde{\alpha} = D_\infty$. In the B field we expect $\tilde{\alpha} \approx 2.5$ (see Fig. 7). Taking a line section through the maximal peak in B, as pictured in the upper panel of Fig. 9, we fitted the peak to this functional form and got reasonable agreement as shown in Fig. 9. We thus conclude that it is very tempting to retain the usual interpretation of D_q being related to the existence of singularities. The surprising consequence is that even at the smallest scales our D_q are smaller than 3. This indicates that singularities appear to be sharp even at scales around the Kolmogorov cutoff. In fact, our results indicate that in the dissipative regime the near singularities are abundant and not space filling. Note that Frisch and Vergassola [23] have also considered corrections to Kolmogorov scaling and the possibility of strong singularities in the region of the viscous cutoff.

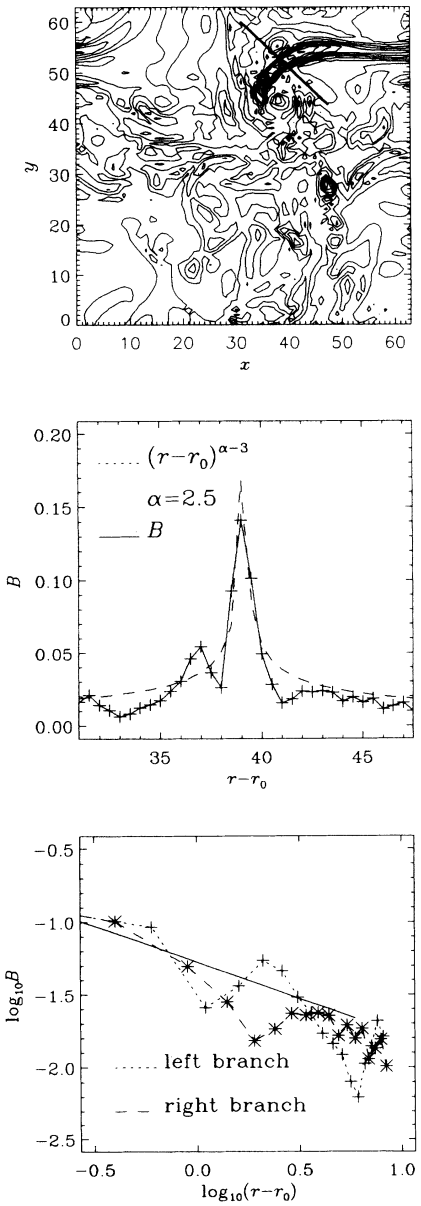

FIG. 9. Upper panel: Contours of B in a horizontal cross section. The heavy line indicates a cut through the maximum value of B. Middle panel: Cross section of B (solid line) and fit to $|\mathbf{r}-\mathbf{r}_0|^{\tilde{\alpha}-3}$, with $\tilde{\alpha} = D_\infty$, along the line indicated in the upper panel. Lower panel: log-log plot of the left- and right-hand branches of B (dashed lines) together with the fit (solid line).

It is noteworthy that our numerical analysis indicates that in all the cases that we examined the most probable index α (with respect to the measures defined in the computation for each field) is always smaller than 3. This can be seen by finding the diagonal tangent $f = \alpha$ to the $f(\alpha)$ curves. This diagonal is tangent to the curve at the most probable α, which is also $\alpha(q = 1)$ which is related to the information dimension D_1. On the other hand, the index α which is exhibited by most of the boxes, i.e., where $f = 3$, turns out to be larger than 3. This $\alpha(q = 0)$ is the most abundant with respect to the uniform measure. These numerical results indicate that the comparatively rare intense events are compensated by very many regions in which the fields are rather "rarified" with a scaling index that is larger than 3. It would be worthwhile to develop an understanding of this finding. It appears that the experimental results of Sreenivasan point to the same direction, and in his one-dimensional "cuts" through the data the most probable α is smaller than 1 [25].

VII. THE CAPACITY DIMENSION

The capacity dimension D_θ is obtained from the scaling of $N(r;\theta)$, where $N(r;\theta)$ is defined by

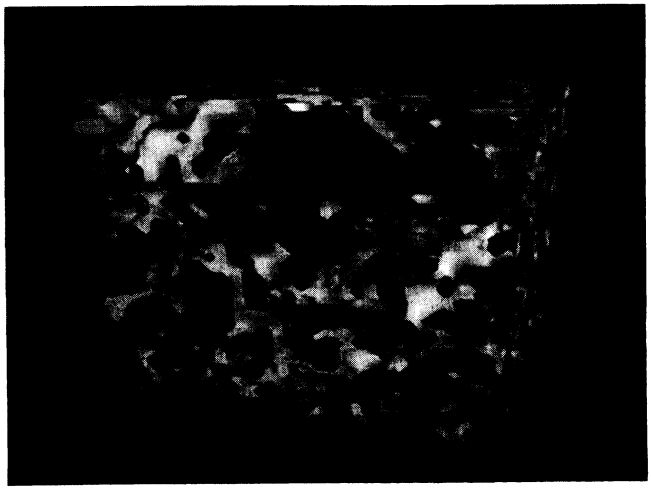

FIG. 10. Visualization of the set of subvolumes of length $r = 8$ mesh sizes needed to cover 70% of the total field w.

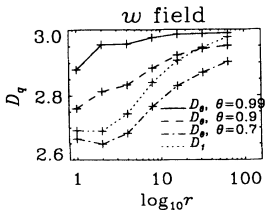

FIG. 11. D_θ for $\theta = 0.7$, 0.9, and 0.99 and D_1 for w in hydrodynamic turbulence.

$$\sum_{i=1}^{N(r,\theta)} p_i = \theta. \tag{15}$$

Here, θ is the fraction of the field that is contained in the minimum number of subvolumes $N(r;\theta)$. In Fig. 10 we visualize the set of subvolumes of length $r = 8$ mesh sizes needed to cover 70% of the total field w.

Of course, since $\theta = 1$ corresponds to the entire space, we have $D_{\theta=1} = D_0$. It has been argued that for typical fractal measures $\lim_{\theta\to 1} D_\theta = D_1$. This has been demonstrated for simple strange attractors like the Henon map [24]. Thus, we expect a discontinuity of D_θ between $\theta < 1$ and $\theta = 1$. In order to check this in our cases we determine D_θ for w; see Fig. 11. We find that D_θ approaches $D_0 = 3$ continuously as $\theta \to 1$. Our data therefore do not satisfy $\lim_{\theta\to 1} D_\theta = D_1$. Both for MHD and hydrodynamic turbulence D_1 is closest to $D_{\theta\approx 0.90}$. It is not clear, however, whether the reason why we do not see a discontinuity of D_θ as $\theta \to 1$ is due to the fact that the Reynolds numbers in our simulations are only modest, so that the multifractal picture holds only on a limited range of scales.

VIII. TWO-DIMENSIONAL SLICES

Recently, the fractal dimensions of solar granulation and solar magnetic fields have been estimated. For the solar granulation there is a crossover from $D \approx 1.3$ at small scales to 1.9 at large scales [12], and for the magnetic field $D \approx 1.54 \pm 0.03$ at small scales with a crossover to 2 at large scales [15]. It is not however appropriate to directly interpret the observed fractal dimension of solar MHD turbulence in terms of the theory and models presented here, because the observations' resolution is limited to about 100 km. This is much larger than the Kolmogorov cutoff $\ell_D \sim L\,\mathrm{Re}^{-3/4}$. In the upper parts of the Sun $\ell_D \approx 3$ cm, if we use $\mathrm{Re}=10^{10}$ and $L \approx 1000$ km for the integral scale L. Thus, we do not expect that the crossover found in the observations has anything to do with the crossover observed in the numerical data.

Moreover, the observational data only represent a two-dimensional slice of the field at the solar surface. Under isotropic conditions one would expect that the dimension obtained in such a way is smaller by one than the dimension obtained from analyzing three-dimensional data. This is true at least for homogeneous fractals (including nonfractal objects). Our results allow us to test this and to infer the possible sensitivity to anisotropies necessarily present in convection. We find that the generalized dimension depends slightly on the depth at which the slice is taken, but it lies in all cases roughly between 1.8 and 1.9; see Fig. 12. Our results therefore suggest that the codimension obtained from two-dimensional slices is somewhat smaller than for the full three-dimensional data. In contrast, for the fractal dimension of level sets in two-dimensional slices we find considerable dependence on depth; see Fig. 13 where we show $D(r)$ for different layers. In order to improve the statistics we have averaged $C(r)$ over five neighboring layers. In the lower parts (e.g., for $n = 21 - 25$, where n is the vertical mesh layer and n increases downwards) we find a crossover behavior compatible with the expected one from $D = 1$ at small scales to $D = 1.7$ at large scales. In the upper layers, however, the level sets do not seem to be smooth at the smallest scales.

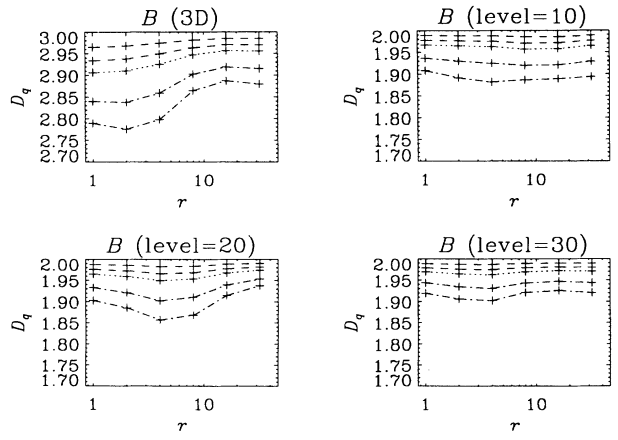

FIG. 12. Comparison of the generalized dimension of B obtained from the full three-dimensional data with that obtained from two-dimensional slices taken at three different heights.

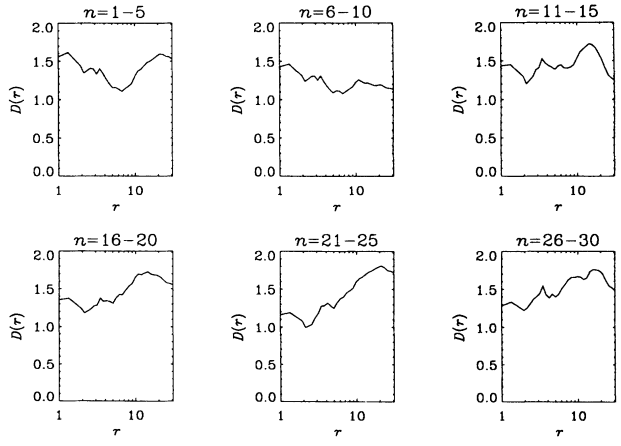

FIG. 13. Fractal dimension of level sets in two-dimensional slices at different layers (e.g., $n = 1 - 5$ refers to the upper layers and $n = 26 - 30$ to the lower ones).

IX. SUMMARY AND CONCLUSIONS

To summarize this paper we reiterate the three results that seem central to our investigation.

(i) The fractal geometry of level sets of all the different fields seems to present a universal behavior; it crosses from a smooth two-dimensional scaling (at the same typical scale λ^*) to a fractal behavior with dimension close to 2.7. This is in good agreement with our theoretical expectation.

(ii) The various fields fall into two classes that we would like to designate class S and class N: fields in class S are strongly stretched locally whereas fields in class N are not. Fields in class S exhibit multifractal behavior and fields in class N do not.

(iii) The multifractal behavior is seen best in the dissipative range. The near singularities seem to be well resolved down to the Kolmogorov scale. There is a reasonable agreement between the values of D_∞ and the direct picture of the highest peak in the simulation.

All the results obtained here are in qualitative agreement with a picture of weak near singularities which are riding on a rather uniform background. In some sense the scaling properties can be thought of as coming from two "phases" in equilibrium. One phase has standard, regular behavior, and the other phase is dominated by rare but powerful events that at this value of the Reynolds number are only felt at small scales. This picture seems to be nicely characterized with the tools of multifractal analysis. We should note however that, before we generate a good understanding of the theoretical aspects of this picture, all the numerical results on D_q and $f(\alpha)$ should be treated with utmost care and considered as indicative only.

It is tempting to offer some conjectures about the effect of singularities on the scaling behavior in the inertial range. It is quite possible that even at much higher Reynolds numbers (Re$\gg 10^3$) one would need to go down to relatively small scales in order to see the singularities in the multifractal analysis. Thus, it is likely that at intermediate values of the Reynolds number the inertial range would be partly "Kolmogorov-like" (for larger values of r) and partly "anomalous" (for smaller values of r). If so, one should not attempt to fit a single scaling exponent throughout the inertial range, but rather find a Re-dependent crossover between regular and multifractal scaling. Further experimental evidence is needed before one can make definite conclusions.

ACKNOWLEDGMENTS

We acknowledge useful discussions about singularities and multifractality with Jean-Pierre Eckmann, K.R. Sreenivasan, and Dennis Sullivan. This work was supported in part by the German-Israeli Foundation (A.B. and I.P.), the Einstein Center for Theoretical Physics at the Weizmann Institute of Science (A.B.), and the US-Israel Binational Science Foundation (I.P.).

[1] P. Constantin and I. Procaccia, Phys. Rev. A (to be published).
[2] L. Cafarelli, R. Kohn, and L. Nirenberg, Comments Pure Appl. Math. **35**, 71 (1982).
[3] C. Meneveau and K. R. Sreenivasan, Phys. Rev. Lett. **59**, 1424 (1987); Nucl. Phys. B (Proc. Suppl.) **2**, 49 (1987).
[4] R. A. Prasad, C. Meneveau, and K. R. Sreenivasan, Phys. Rev. Lett. **61**, 74 (1988).
[5] P. Constantin, I. Procaccia, and K. R. Sreenivasan, Phys. Rev. Lett. **67**, 1739 (1991).
[6] I. Procaccia, A. Brandenburg, M. H. Jensen, and A. Vincent, Europhys. Lett. **19**, 183 (1992).
[7] G. K. Batchelor, Proc. R. Soc. London, Ser. A **201**, 405 (1950).
[8] E. D. Siggia, J. Fluid Mech. **107**, 375 (1981); Z.-S. She, E. Jackson, and S. A. Orszag, Nature **344**, 226 (1990).
[9] A. Vincent and M. Meneguzzi, J. Fluid Mech. **225**, 1 (1991).
[10] S. Kida, S. Yanase, and J. Mizushima, Phys. Fluids A **3**, 457 (1991).
[11] Å. Nordlund, A. Brandenburg, R. L. Jennings, M. Rieutord, J. Ruokolainen, R. F. Stein, and I. Tuominen, Astrophys. J. **392**, 647 (1992).
[12] P. N. Brandt, R. Greimel, E. Guenther, and W. Mattig, in *Applying Fractals in Astronomy*, edited by A. Heck and J. M. Perdang, Lecture Notes in Physics Vol. m3 (Springer-Verlag, Berlin, 1991), p. 77.
[13] A. A. Ruzmaikin, D. D. Sokoloff, and T. Tarbell, in *The Sun and Cool Stars: Activity, Magnetism, Dynamos*, edited by I. Tuominen, D. Moss, and G. Rüdiger, Lecture Notes in Physics Vol. 380 (Springer-Verlag, Berlin, 1991), p. 140.
[14] J. Finn and E. Ott, Phys. Rev. Lett. **60**, 760 (1988).
[15] C. J. Schrijver, C. Zwaan, A. C. Balke, T. D. Tarbell, and J. K. Lawrence, Astron. Astrophys. **253**, L1 (1992).
[16] G. W. Simon, A. M. Title, and N. O. Weiss, Astrophys. J. **375**, 775 (1991).
[17] A. Vincent and M. Meneguzzi, J. Fluid Mech. (to be published).
[18] R. Ramshankar and J. P. Gollub, Phys. Fluids A **3**, 1344 (1991).
[19] H. G. E. Hentschel and I. Procaccia, Physica D **8**, 435 (1983).
[20] T. C. Halsey, M. H. Jensen, L. P. Kadanoff, I. Procaccia, and B. I. Shraiman, Phys. Rev. A **33**, 1141 (1986).
[21] A. N. Kolmogorov, J. Fluid Mech. **13**, 82 (1962); B. B. Mandelbrot, *ibid.* **62**, 331 (1974).
[22] S. Kida and K. Ohkitani, Phys. Fluids A **4**, 1018 (1992).
[23] U. Frisch and M. Vergassola, Europhys. Lett. **14**, 439 (1991).
[24] J. D. Farmer, E. Ott, and J. A. Yorke, Physica D **7**, 153 (1983).
[25] K. R. Sreenivasan (private communication).

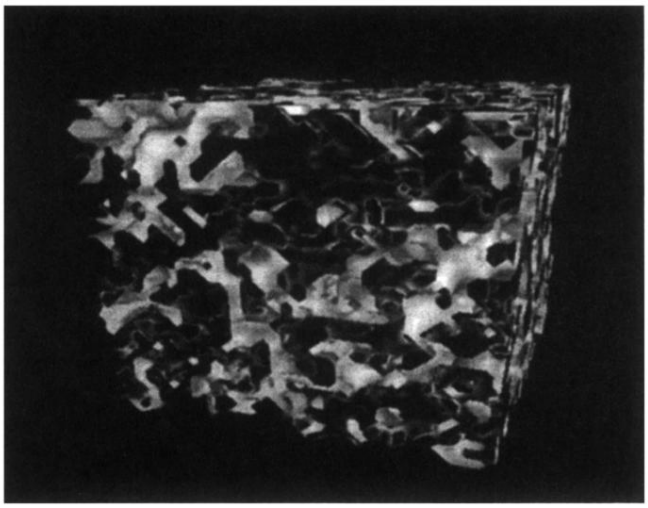

FIG. 10. Visualization of the set of subvolumes of length $r = 8$ mesh sizes needed to cover 70% of the total field w.